

UC Davis

UC Davis Previously Published Works

Title

Real-time, label-free characterization of oligosaccharide-binding proteins using carbohydrate microarrays and an ellipsometry-based biosensor

Permalink

<https://escholarship.org/uc/item/75w6f35v>

Journal

Instrumentation Science & Technology, 45(5)

ISSN

1073-9149

Authors

Sun, Yung-Shin
Zhu, XD

Publication Date

2017-09-03

DOI

10.1080/10739149.2016.1278017

Peer reviewed



Published in final edited form as:

Instrum Sci Technol. 2017 ; 45(5): 506–524. doi:10.1080/10739149.2016.1278017.

Real-time, label-free characterization of oligosaccharide-binding proteins using carbohydrate microarrays and an ellipsometry-based biosensor

Yung-Shin Sun¹ and X. D. Zhu²

¹Department of Physics, Fu-Jen Catholic University, New Taipei City, Taiwan

²Department of Physics, University of California at Davis, Davis, CA, USA

Abstract

Carbohydrates present on cell surfaces mediate cell behavior through interactions with other biomolecules. Due to their structural complexity, diversity, and heterogeneity, it is difficult to fully characterize a variety of carbohydrates and their binding partners. As a result, novel technologies for glycomics applications have been developed, including carbohydrate microarrays and label-free detection methods. In this paper, we report using the combination of oligosaccharide microarrays and the label-free oblique-incidence reflectivity difference (OI-RD) microscopy for real-time characterization of oligosaccharide binding proteins. Aminated human milk oligosaccharides were immobilized on epoxy-coated glass substrates as microarrays for reactions with Family 1 of solute binding proteins from *Bifidobacterium longum* subsp. *infantis* (*B. infantis*). Binding affinities of these protein-oligosaccharide interactions showed preferences of Family 1 of solute binding proteins to host glycans, which helps in characterizing the complex process of human milk oligosaccharides foraging by *B. infantis*.

Keywords

label-free biosensor; oblique-incidence reflectivity difference (OI-RD); carbohydrate microarray; solute binding proteins; real-time kinetics

INTRODUCTION

Carbohydrates play important roles in a wide range of biochemical interactions because all cells are surrounded by layers mostly composed of oligo- and polysaccharides [1, 2]. These sugars act as part of the protective layers defending cells against harmful physical impact. Moreover, through interactions with other biomolecules, they regulate cell behaviors, especially those involving surfaces such as cell-cell interactions [3, 4], cell adhesion [5, 6], and cell motility [7, 8]. Certain protein-carbohydrate interactions are crucial to biological processes such as metastasis [9], immune response [10, 11], and pathogen-host infections [12]. Considering the infectious virus as an example, the virus uses surface glycoprotein hemagglutinin (HA) to attach itself to a host cell surface and initiate transfer of viral genome

into infected cell through binding to sialosides on the surface of the cell [13, 14]. Abnormal expression of carbohydrates is related to several diseases including cancer, and as a result, they are believed to be important drug candidates [15–17].

In modern glycobiology, it remains a big challenge to fully characterize a variety of carbohydrates and their binding partners because of several reasons. First, the structures of carbohydrates are usually complex, diverse, and heterogeneous [18, 19]. Carbohydrate molecules (monosaccharides, oligosaccharides, and polysaccharides) consist of different numbers of sugar units, ranging from one to as many as 500,000 monosaccharide units. Second, unlike nucleic acids and proteins, the synthesis of carbohydrates is not template driven, meaning that multiple enzymes are required in a complex pathway of biosynthesis. Thirdly, the interactions between carbohydrates and other biomolecules are usually of low affinities. For example, due to shallow binding pockets of lectins (carbohydrate-binding proteins), the affinities of these proteins to carbohydrates vary over a wide range (equilibrium dissociation constant $\sim 10^{-3}$ to 10^{-6} M) [20, 21] and are relatively weak compared with antibody-antigen reactions (equilibrium dissociation constant $\sim 10^{-8}$ to 10^{-12} M) [22, 23]. Finally, many important functions and roles of carbohydrates have not been fully understood. Comparing to genomics and proteomics, the area of glycomics has just been actively studied in recent years.

To overcome this challenge, modern technologies for glycomics have been proposed and developed [24, 25], including carbohydrate microarrays and label-free biosensors. Microarrays are high-throughput platforms for parallel assays of hundreds to thousands of distinct biomolecular interactions [26, 27]. Following the successful development and progress in DNA microarrays [28, 29] and protein microarrays [30, 31], carbohydrate microarrays have also become valuable tools in glycobiology [13, 32–34]. Carbohydrate microarrays, consisting of distinct glycans immobilized on solid substrates, serve for simultaneously detecting binding reactions of proteins, viruses, and cells to a large number of glycans under identical conditions. There are several ways to efficiently immobilize mono-, di-, oligo-, and polysaccharides on functionalized solid substrates while maintaining their innate functionalities [35].

For example, unmodified carbohydrates can be directly immobilized on either hydrazidecoated glass slides [36] or nitrocellulose-coated glass slides [37]. Amine- and maleimidemodified carbohydrates can be covalently attached on *N*-hydroxysuccinimide- and thiolactivated glass slides, respectively [38, 39]. Traditionally, characterization of bindings between surface-immobilized carbohydrates and solution-phase probes involves some forms of fluorescence-based methods where probes are labeled with fluorescent tags [38, 40, 41]. However, labeling probes, especially proteins, inevitably changes their binding properties in uncharacterized ways [42, 43]. Therefore, a number of label-free, optical biosensors based on surface plasma resonance (SPR) [44, 45] and ellipsometry [46, 47] have been developed for measurements of carbohydrate-biomolecule interactions in a high-throughput manner. We recently developed the oblique-incidence reflectivity difference (OI-RD) microscopy for label-free detection of biomolecular interactions between solution-phase analyte and surface-immobilized microarrays [48–50]. This ellipsometry-based OI-RD microscope is

suitable for both real-time measurements of binding curves and end-point imaging of biomolecular microarrays [51, 52].

Bifidobacterium longum subsp. *infantis* (*B. infantis*), one of the earliest colonizers of the gastrointestinal tract of infants, is characterized by its foraging capacity of human milk oligosaccharides [53]. The building blocks of human milk oligosaccharides contain Dglucose, D-galactose, *N*-acetylglucosamine, L-fucose, and sialic acid [54]. To utilize these carbon sources, *B. infantis* have specific glycoside hydrolases to promote the hydrolysis of glycosidic bonds in complex carbohydrates and the following import of these processed glycans. The genome sequence of *B. infantis* showed an overabundance of the Family 1 of solute binding proteins, a portion of bacterial ATP-binding cassette transporters (the so-called ABC transporters) and related to the processing of oligosaccharides [53]. Therefore, the characterization of these solute binding proteins, especially in their interactions with human milk oligosaccharides, is crucial to understanding the molecular mechanisms involved in the adaptations of *B. infantis* to the gastrointestinal tract of infants.

In this paper, we report the characterization of these oligosaccharide binding proteins using the combination of carbohydrate microarrays and OI-RD microscopy. 12 human milk oligosaccharides with different mass-to-charge (m/z) ratios were profiled and separated using the high-performance liquid chromatography – mass spectrometry (HPLC-MS) chip technology described in the literature [55, 56]. These human milk oligosaccharides, together with 4 control oligosaccharides, were aminated for immobilization on epoxy-coated glass substrates as carbohydrate microarrays. These microarrays were further reacted with *B. infantis* Family 1 of solute binding proteins for determining the binding affinities of specific protein-oligosaccharide interactions. The results indicate that Family 1 of solute binding proteins have different affinities to host oligosaccharides, and these preferences are important in characterizing the complex process of human milk oligosaccharides foraging by *B. infantis*.

EXPERIMENTAL

Aminated Oligosaccharides

8 human milk oligosaccharides (#1 through #8) with different m/z (mass to charge) ratios were analyzed and separated from human milk oligosaccharides as described in the literature [55, 56]. 4 known oligosaccharides were purchased from Sigma-Aldrich (St. Louis, MO) (#9, #10, and #12) and Dextra Labs (Reading, UK) (#11). All oligosaccharides were aminated and dissolved in 1× phosphate buffered saline as targets for microarray printing. The mass (aminated and neutral m/z ratios) and composition (numbers of hexose, *N*-acetylhexoseamine, deoxyhexose, and *N*-acetylneuraminic acid groups) of these aminated oligosaccharides were analyzed by mass spectrometry and the results are listed in Table 1.

Preparation of Carbohydrate Microarrays and Procedure of Subsequent Reactions

12 aminated oligosaccharides were dissolved in 1× phosphate buffered saline to 100 μ M for microarray printing. Using an OmniGrid 100 contact-printing arrayer (Digilab, Holliston, MA), 2 copies of each of the 12 oligosaccharides were immobilized on epoxycoated glass

slides (CEL Associates, Pearland, TX). By contact printing 10 times at each location, a sufficient volume of target solution was deposited over an area of around 100 μm in diameter. The microarray-bearing slides were stored as printed in slide boxes for at least 24 hrs before further processing. Subsequently, the slide was assembled into a flow cell and washed with a flow of 1 \times phosphate buffered saline for 5 min. To block the remaining free epoxy groups on the glass surface from non-specific reactions with protein probes, the printed microarray was treated with a flow of bovine serum albumin solution at 8.3 μM in 1 \times phosphate buffered saline for 10 min and then washed with a flow of 1 \times phosphate buffered saline for 5 min. The 1 \times phosphate buffered saline buffer in the flow cell was replaced with a solution of protein probes at a desired concentration for the association phase, and finally the solution was switched back to 1 \times phosphate buffered saline buffer for the dissociation phase.

Protein Probes

Family 1 of solute binding proteins from *B. infantis* were cloned and expressed as described in details in references [53, 57]. 6 glutathione S-transferase-tagged Family 1 of solute binding proteins with different genome sequences were dissolved in 1 \times phosphate buffered saline to desired concentrations and reacted with the human milk oligosaccharide microarray. The molecular weight of these glutathione S-transferasetagged proteins was estimated to be around 125 kDa (95 kDa for protein + 30 kDa for glutathione S-transferase tag).

OI-RD Microscopy for Label-Free Carbohydrate Microarray Detection

The oblique-incidence reflectivity difference scanning microscope used in the present work was described in earlier publications [42, 51, 52]. It employed a He-Ne laser at a wavelength of 633 nm for illumination. We measured the OR-RD signal defined as $(r_p - r_{p0})/r_{p0} - (r_s - r_{s0})/r_{s0} \equiv \Delta_p - \Delta_s$, where r_{p0} and r_{s0} are the complex reflectivities of the bare glass surface, r_p and r_s are the reflectivities of the glass surface covered with immobilized carbohydrate layer [58]. The physical properties of a surface-bound biomolecular layer are related to $\Delta_p - \Delta_s$ by [50, 59]

$$\Delta_p - \Delta_s \cong -i \left[\frac{4\pi\epsilon_s (\tan \phi_{\text{inc}})^2 \cos \phi_{\text{inc}}}{\epsilon_0^{1/2} (\epsilon_s - \epsilon_0) (\epsilon_s / \epsilon_0 - (\tan \phi_{\text{inc}})^2)} \right] \frac{(\epsilon_d - \epsilon_s)(\epsilon_d - \epsilon_0) \Theta \left(\frac{d}{\lambda} \right)}{\epsilon_d}, \quad (1)$$

where ϕ_{inc} is the incidence angle of the illumination laser beam and ϵ_0 , ϵ_d , and ϵ_s are the respective optical constants of the aqueous ambient, the biomolecular layer (e.g., printed targets and/or captured probes), and the glass slide at 633 nm. In our present study, $\phi_{\text{inc}} = 65^\circ$, $\epsilon_s = 2.307$ for glass slide, $\epsilon_0 = 1.788$ for aqueous buffer, and $\epsilon_d = 2.031$ for packed biomolecules in solution [50]. In this work, d is the thickness of the biomolecular layer and Θ is the coverage of the layer, defined as the ratio of the area covered by the layer to the total available area. Θd and thus $\Delta_p - \Delta_s$ is proportional to the surface mass density (Γ) of the immobilized molecular layer.

The OI-RD image of a carbohydrate microarray was acquired by moving the sample stage two-dimensionally with a linear step size of 20 μm in both directions. To acquire real-time binding curves, we measured the OI-RD signals of one pixel from a printed spot (target pixel) and one pixel from the unprinted region adjacent to the target (reference pixel), and took the difference as one time point of the binding curve. This was repeated at a time interval shorter than the characteristic time of the reaction. This procedure reduced the contribution of the drift in the optical system to the binding curve measurement.

Model for Analysis of Binding Curves

Rate constants and equilibrium dissociation constants for protein-carbohydrate interactions were deduced by globally fitting a set of binding curves, each of which corresponded to a concentration $[c]$ of the protein, to the 1-to-1 Langmuir reaction model [45, 60, 61]. In this model, the surface mass density $\Gamma(t)$ of the captured protein evolves during the association phase of the binding reaction as follows:

$$\Gamma(t) = \frac{\Gamma_{MAX}k_{on}[c]}{k_{on}[c] + k_{off}} \left(1 - e^{-(k_{on}[c] + k_{off})t} \right) \quad 0 < t < t_0; \quad (2)$$

during the subsequent dissociation phase, i.e., after the probe solution is replaced with 1 \times phosphate buffered saline buffer at $t = t_0$,

$$\Gamma(t) = \frac{\Gamma_{MAX}k_{on}[c]}{k_{on}[c] + k_{off}} \left(1 - e^{-(k_{on}[c] + k_{off})t_0} \right) e^{-k_{off}(t-t_0)} \quad t > t_0 \quad (3)$$

where Γ_{MAX} is the maximum amount of probes that can be captured by the immobilized carbohydrate targets and k_{on} and k_{off} are the association and dissociation rate constants, respectively. The equilibrium dissociation constant of a binding reaction is defined as $K_D = k_{off}/k_{on}$. Since the OI-RD signal (Eq. (1)) is proportional to $\Gamma(t)$, we expect the optical signal to vary in time as

$$\Delta_p - \Delta_s = \gamma \frac{k_{on}[c]}{k_{on}[c] + k_{off}} \left(1 - e^{-(k_{on}[c] + k_{off})t} \right) \quad \left(Association \right) \quad 0 < t < t_0; \quad (4)$$

(Association) $0 < t < t_0$;

$$\Delta_p - \Delta_s = \gamma \frac{k_{on}[c]}{k_{on}[c] + k_{off}} \left(1 - e^{-(k_{on}[c] + k_{off})t_0} \right) e^{-k_{off}(t-t_0)} \quad \left(Dissociation \right) \quad t > t_0. \quad (5)$$

Here, Γ , one of the fitting parameters, is proportional to Γ_{MAX} .

RESULTS AND DISCUSSION

OI-RD Images of Carbohydrate Microarrays

Figure 1 shows the OI-RD image of a carbohydrate microarray after printing. The spot size is approximately 100 μm in diameter, and the center-to-center spacing is about 200 μm . The corresponding layout of the microarray is illustrated to the right. The intensity bar is not shown because the OI-RD signals of this dry microarray are oversaturated due to surface-accumulated salts and excess oligosaccharide targets. To remove these precipitates, the microarray was first washed with 1 \times phosphate buffered saline. The OIRD image of the carbohydrate microarray after washing is shown in Figure 2a (with the microarray still in contact with 1 \times phosphate buffered saline). After washing, all target spots are visible with OI-RD signals of 1×10^{-3} to 2×10^{-3} . These correspond to surface mass densities Γ of 1.7×10^{-7} to 3.4×10^{-7} g/cm² [51] and the microarray was blocked with a bovine serum albumin solution of 8.3 μM for 10 min. Figure 2b shows the differential OI-RD image of the microarray, obtained by subtracting the image taken after washing from the image taken after blocking and subsequent washing (with the microarray still in contact with 1 \times phosphate buffered saline). After blocking, free bovine serum albumin molecules bound to unprinted regions, and all target spots became darker as a result of an increased background signal. It has been shown that under this blocking concentration (8.3 μM of bovine serum albumin), a side-on monolayer of fully packed bovine serum albumin molecules ($\Gamma \sim 4 \times 10^{-7}$ g/cm²) was accumulated on the surface [51]. Therefore, all surface-immobilized oligosaccharides must have less than a side-on monolayer of fully packed bovine serum albumin molecules.

Binding Kinetics of Solute Binding Proteins to Oligosaccharides

The carbohydrate microarray containing 12 oligosaccharides was reacted with 6 different Family 1 of solute binding proteins at desired concentrations. One fresh microarray was used in each reaction condition (one protein at one concentration). Figure 3 shows the association-dissociation curves for solute binding protein 2344 reacting with 12 oligosaccharides. The concentrations of proteins are 236 (red), 472 (green), and 944 (blue) nM. At $t = 0$, the aqueous ambient in contact with the microarray was changed from 1 \times phosphate buffered saline to a protein solution at a desired concentration. At $t = 1800$ s, the ambient was restored back to 1 \times phosphate buffered saline for dissociation. The binding curves in each panel were fitted globally to the 1-to-1 Langmuir reaction model (Eq. (4) and (5)) with k_{on} , k_{off} , and Γ being the global fitting parameters. The fits are shown in dotted lines in the figure and the equilibrium dissociation constants are listed in Table 2.

From Figure 3, it is clear that solute binding protein 2344 reacted with all 12 oligosaccharides, but the OI-RD signals were relatively weak (1×10^{-4} to 8×10^{-4}) compared with those of printed targets (1×10^{-3} to 2×10^{-3}). These signals correspond to only about one-tenth of a side-on monolayer of fully packed immunoglobulin G molecules (an antibody isotype with a molecular weight of 150 kDa) [51]. Also, except for #2, #8, and #10, the dissociation phase was not obvious so that dissociation rate constants and equilibrium dissociation constants have no values but only upper limits [51, 62]. For example, the equilibrium dissociation constant of solute binding protein 2344 binding to #1

is less than 42 nM. In summary, the equilibrium dissociation constants of solute binding protein 2344 binding to oligosaccharides range from 6 nM (#6, the strongest binding affinity) to 79 nM (#10, the weakest binding affinity), and these values are close to what have been reported in lectin-oligosaccharide reactions [62].

Figure 4, 5, 6, 7, and 8 show the association-dissociation curves of 12 oligosaccharides reacting with solute binding protein 2352, solute binding protein 2350, solute binding protein 0343, solute binding protein 2177, and solute binding protein 0883, respectively. The colors indicate different probe concentrations as reported in the figure captions. After globally fitting the curves in each panel, the equilibrium dissociation constants of all reactions are listed in Table 2. Solute binding protein 2352 reacted with #1, #5, #6, #7, #9, #10, #11, and #12 with small OI-RD signals (1×10^{-4} to 2×10^{-4} , corresponding to about one-thirtieth of a side-on monolayer of fully packed immunoglobulin G molecules). It has the strongest binding affinity (the smallest equilibrium dissociation constant for 11 nM) to #1 and the weakest binding affinity (the largest equilibrium dissociation constant of approximately 150 nM) to #7. Solute binding protein 2350 reacted with #1, #2, #3, #5, #6, #7, #9, #10, #11, and #12 with OI-RD signals of 1×10^{-4} to 8×10^{-4} (corresponding to approximately one-tenth of a side-on monolayer of fully packed immunoglobulin G molecules).

As shown in Figure 5, some dissociation curves were missing due to large drift in this set of reactions. It has the strongest binding affinity (the smallest equilibrium dissociation constant of 12 nM) to #7 and the weakest binding affinity (the largest equilibrium dissociation constant of 173 nM) to #10. Solute binding protein 0343 reacted with all oligosaccharides except #8 with relatively higher OI-RD signals (up to 2×10^{-3} , corresponding to about one-half of a side-on monolayer of fully packed immunoglobulin G molecules). It has the strongest binding affinity (the smallest equilibrium dissociation constant of 8 nM) to #12 and the weakest binding affinity (the largest equilibrium dissociation constant of 72 nM) to #6.

Solute binding protein 2177 reacted only with #1, #4, and #10 with OI-RD signals of 1×10^{-4} to 4×10^{-4} (corresponding to about one-twentieth of a side-on monolayer of fully packed immunoglobulin G molecules). It has the strongest binding affinity (the smallest equilibrium dissociation constant of 3 nM) to #4 and #10, and the weakest binding affinity (the largest equilibrium dissociation constant of 70 nM) to #1. Solute binding protein 0883 reacted with #1, #2, #3, #6, #7, #9, and #10 with weak OI-RD signals (less than 1×10^{-4} , corresponding to about one-fortieth of a side-on monolayer of fully packed immunoglobulin G molecules). It has the strongest binding affinity (the smallest equilibrium dissociation constant of 9 nM) to #1 and the weakest binding affinity (the largest equilibrium dissociation constant of 225 nM) to #2.

From Figures 3, 4, 5, 6, 7, and 8 and Table 2, oligosaccharide binding proteins Family 1 of solute binding proteins from *B. infantis* show specific preferences for host glycans. These protein-oligosaccharide interactions have different binding intensities (different OI-RD signals) and affinities (different equilibrium dissociation constants). The next step will be to study the dependence of these preferences on the structures of surface-immobilized

oligosaccharides. This will help in characterizing the complex process of oligosaccharides, particularly human milk oligosaccharides, foraging by *B. infantis*.

CONCLUSIONS

Carbohydrate microarrays are high-throughput assay platforms for characterizing and profiling protein-carbohydrate interactions that are numerous and complex. Label-free, real-time, and *in-situ* detection of protein binding reactions with carbohydrate microarrays have advantages over fluorescence-based methods by preserving the innate properties of proteins and offering the capability of measuring association-dissociation curves and thus directly yielding reaction kinetics. The latter not only enhances the efficiency and relevance of carbohydrate microarray platforms, but also makes the platform free of density variation of immobilized targets. Using the OI-RD scanning microscope as a versatile label-free biosensor of carbohydrate microarrays, we characterized different oligosaccharide binding proteins by studying their binding affinities to surface-immobilized glycans including human milk oligosaccharides. We found that Family 1 of solute binding proteins from *B. infantis* reveal preferences for host oligosaccharides, and the structural difference in carbohydrates can induce large changes in binding affinity constants in terms of equilibrium dissociation constant. Therefore, the combination of a label-free OI-RD biosensor and carbohydrate microarrays can be utilized to profile and characterize selected proteins and their interactions with glycans.

ACKNOWLEDGEMENTS

This work was financially supported by NIH-R01-HG003827 (X.D. Zhu) and Taiwan MOST 105-2112-M-030-002-MY2 (Y.S. Sun). The authors want to thank to Dr. David A. Mills for providing the protein probes and Dr. Carlito Lebrilla for providing the oligosaccharides.

REFERENCES

1. Roseman S, Reflections on glycobiology. *J Biol Chem* 2001, 276, (45), 41527–42. [PubMed: 11553646]
2. Horlacher T; Seeberger PH, Carbohydrate arrays as tools for research and diagnostics. *Chem Soc Rev* 2008, 37, (7), 1414–1422. [PubMed: 18568167]
3. Adachi T; Sato C; Kishi Y; Totani K; Murata T; Usui T; Kitajima K, Membrane microdomains from early gastrula embryos of medaka, *Oryzias latipes*, are a platform of E-cadherin- and carbohydrate-mediated cell-cell interactions during epiboly. *Glycoconj J* 2009, 26, (3), 285–99. [PubMed: 18766437]
4. Crocker PR; Feizi T, Carbohydrate recognition systems: functional triads in cell-cell interactions. *Curr Opin Struct Biol* 1996, 6, (5), 679–91. [PubMed: 8913692]
5. Miura R; Ethell IM; Yamaguchi Y, Carbohydrate-protein interactions between HNK-1-reactive sulfoglucuronyl glycolipids and the proteoglycan lectin domain mediate neuronal cell adhesion and neurite outgrowth. *J Neurochem* 2001, 76, (2), 413–24. [PubMed: 11208904]
6. Lorenz B; Alvarez de Cienfuegos L; Oelkers M; Kriemen E; Brand C; Stephan M; Sunnick E; Yuksel D; Kalsani V; Kumar K; Werz DB; Janshoff A, Model system for cell adhesion mediated by weak carbohydrate-carbohydrate interactions. *J Am Chem Soc* 2012, 134, (7), 3326–9. [PubMed: 22296574]
7. Kahsai AW; Cui J; Kaniskan HU; Garner PP; Fenteany G, Analogs of tetrahydroisoquinoline natural products that inhibit cell migration and target galectin-3 outside of its carbohydrate-binding site. *J Biol Chem* 2008, 283, (36), 24534–45. [PubMed: 18556657]

8. Chou DK; Zhang J; Smith FI; McCaffery P; Jungalwala FB, Developmental expression of receptor for advanced glycation end products (RAGE), amphoterin and sulfoglucuronyl (HNK-1) carbohydrate in mouse cerebellum and their role in neurite outgrowth and cell migration. *J Neurochem* 2004, 90, (6), 1389–401. [PubMed: 15341523]
9. Krishnan V; Bane SM; Kawle PD; Naresh KN; Kalraiya RD, Altered melanoma cell surface glycosylation mediates organ specific adhesion and metastasis via lectin receptors on the lung vascular endothelium. *Clin Exp Metastasis* 2005, 22, (1), 11–24. [PubMed: 16132574]
10. Ruseva M; Kolev M; Dagnaes-Hansen F; Hansen SB; Takahashi K; Ezekowitz A; Thiel S; Jensenius JC; Gadjeva M, Mannan-binding lectin deficiency modulates the humoral immune response dependent on the genetic environment. *Immunology* 2009, 127, (2), 279–88. [PubMed: 19476514]
11. Lackie AM; Vasta GR, The role of galactosyl-binding lectin in the cellular immune response of the cockroach *Periplaneta americana* (Dictyoptera). *Immunology* 1988, 64, (2), 353–7. [PubMed: 3391649]
12. Schauer R, Sialic Acids, Chemistry, Metabolism and Function. Springer-Verlag: New York, 1982; Vol. 10.
13. Stevens J; Blixt O; Glaser L; Taubenberger JK; Palese P; Paulson JC; Wilson IA, Glycan microarray analysis of the hemagglutinins from modern and pandemic influenza viruses reveals different receptor specificities. *J Mol Biol* 2006, 355, (5), 1143–55. [PubMed: 16343533]
14. Smith AE; Helenius A, How viruses enter animal cells. *Science* 2004, 304, (5668), 237–42. [PubMed: 15073366]
15. Liu CC; Ye XS, Carbohydrate-based cancer vaccines: target cancer with sugar bullets. *Glycoconj J* 2012, 29, (5–6), 259–71. [PubMed: 22669462]
16. Adamo R; Nilo A; Harfouche C; Brogioni B; Pecetta S; Brogioni G; Balducci E; Pinto V; Filippini S; Mori E; Tontini M; Romano MR; Costantino P; Berti F, Investigating the immunodominance of carbohydrate antigens in a bivalent unimolecular glycoconjugate vaccine against serogroup A and C meningococcal disease. *Glycoconj J* 2014, 31, (9), 637–47. [PubMed: 25256065]
17. Seeberger PH; Werz DB, Automated synthesis of oligosaccharides as a basis for drug discovery. *Nat Rev Drug Discov* 2005, 4, (9), 751–763. [PubMed: 16138107]
18. Wang D, Carbohydrate microarrays. *Proteomics* 2003, 3, (11), 2167–75. [PubMed: 14595816]
19. Imai Y; Rosen SD, Direct demonstration of heterogeneous, sulfated O-linked carbohydrate chains on an endothelial ligand for L-selectin. *Glycoconj J* 1993, 10, (1), 34–9. [PubMed: 7689376]
20. Shinohara Y; Hasegawa Y; Kaku H; Shibuya N, Elucidation of the mechanism enhancing the avidity of lectin with oligosaccharides on the solid phase surface. *Glycobiology* 1997, 7, (8), 1201–8. [PubMed: 9455921]
21. Lee YC; Lee RT, Carbohydrate-Protein Interactions: Basis of Glycobiology. *Acc. Chem. Res* 1995, 28, 321–7.
22. Papalia GA; Baer M; Luehrsen K; Nordin H; Flynn P; Myszkas DG, High-resolution characterization of antibody fragment/antigen interactions using Biacore T100. *Anal Biochem* 2006, 359, (1), 112–9. [PubMed: 17027901]
23. Katsamba PS; Navratilova I; Calderon-Cacia M; Fan L; Thornton K; Zhu M; Bos TV; Forte C; Friend D; Laird-Offringa I; Tavares G; Whatley J; Shi E; Widom A; Lindquist KC; Klakamp S; Drake A; Bohmann D; Roell M; Rose L; Dorocke J; Roth B; Luginbuhl B; Myszkas DG, Kinetic analysis of a high-affinity antibody/antigen interaction performed by multiple Biacore users. *Anal Biochem* 2006, 352, (2), 208–21. [PubMed: 16564019]
24. Bertozzi CR; Kiessling LL, Chemical glycobiology. *Science* 2001, 291, (5512), 2357–64. [PubMed: 11269316]
25. Ratner DM; Adams EW; Disney MD; Seeberger PH, Tools for glycomics: mapping interactions of carbohydrates in biological systems. *ChemBiochem* 2004, 5, (10), 1375–83. [PubMed: 15457538]
26. Schena M, Microarray Analysis. John Wiley and Sons: Hoboken, NJ, 2003.
27. MacBeath G, Protein microarrays and proteomics. *Nat Genet* 2002, 32 Suppl, 526–32. [PubMed: 12454649]
28. Lockhart DJ; Winzeler EA, Genomics, gene expression and DNA arrays. *Nature* 2000, 405, (6788), 827–36. [PubMed: 10866209]

29. Ramsay G, DNA chips: state-of-the art. *Nat Biotechnol* 1998, 16, (1), 40–4. [PubMed: 9591254]
30. Zhu H; Bilgin M; Bangham R; Hall D; Casamayor A; Bertone P; Lan N; Jansen R; Bidlingmaier S; Houfek T; Mitchell T; Miller P; Dean RA; Gerstein M; Snyder M, Global analysis of protein activities using proteome chips. *Science* 2001, 293, (5537), 2101–5. [PubMed: 11474067]
31. MacBeath G; Schreiber SL, Printing proteins as microarrays for highthroughput function determination. *Science* 2000, 289, (5485), 1760–3. [PubMed: 10976071]
32. Liang PH; Wu CY; Greenberg WA; Wong CH, Glycan arrays: biological and medical applications. *Curr Opin Chem Biol* 2008, 12, (1), 86–92. [PubMed: 18258211]
33. Huang CY; Thayer DA; Chang AY; Best MD; Hoffmann J; Head S; Wong CH, Carbohydrate microarray for profiling the antibodies interacting with Globo H tumor antigen. *Proc Natl Acad Sci U S A* 2006, 103, (1), 15–20. [PubMed: 16373501]
34. Blixt O; Head S; Mondala T; Scanlan C; Huflejt ME; Alvarez R; Bryan MC; Fazio F; Calarese D; Stevens J; Razi N; Stevens DJ; Skehel JJ; van Die I; Burton DR; Wilson IA; Cummings R; Bovin N; Wong CH; Paulson JC, Printed covalent glycan array for ligand profiling of diverse glycan binding proteins. *Proc Natl Acad Sci U S A* 2004, 101, (49), 17033–8. [PubMed: 15563589]
35. Monzo A.a. G., A., Immobilization Techniques for Mono- and Oligosaccharide Microarrays. *QSAR Comb. Sci* 2006, 25, (11), 1033–1038.
36. Lee MR; Shin I, Facile preparation of carbohydrate microarrays by sitespecific, covalent immobilization of unmodified carbohydrates on hydrazide-coated glass slides. *Org Lett* 2005, 7, (19), 4269–72. [PubMed: 15624964]
37. Wang D; Liu S; Trummer BJ; Deng C; Wang A, Carbohydrate microarrays for the recognition of cross-reactive molecular markers of microbes and host cells. *Nat Biotechnol* 2002, 20, (3), 275–81. [PubMed: 11875429]
38. Liang PH; Wang SK; Wong CH, Quantitative analysis of carbohydrateprotein interactions using glycan microarrays: determination of surface and solution dissociation constants. *J Am Chem Soc* 2007, 129, (36), 11177–84. [PubMed: 17705486]
39. Park S; Shin I, Fabrication of carbohydrate chips for studying proteincarbohydrate interactions. *Angew Chem Int Ed Engl* 2002, 41, (17), 3180–2. [PubMed: 12207382]
40. Oyelaran O; McShane LM; Dodd L; Gildersleeve JC, Profiling human serum antibodies with a carbohydrate antigen microarray. *J Proteome Res* 2009, 8, (9), 4301–10. [PubMed: 19624168]
41. Manimala JC; Roach TA; Li Z; Gildersleeve JC, High-throughput carbohydrate microarray profiling of 27 antibodies demonstrates widespread specificity problems. *Glycobiology* 2007, 17, (8), 17C–23C.
42. Sun YS; Landry JP; Fei YY; Zhu XD; Luo JT; Wang XB; Lam KS, Effect of fluorescently labeling protein probes on kinetics of protein-ligand reactions. *Langmuir* 2008, 24, (23), 13399–405. [PubMed: 18991423]
43. Kodadek T, Protein microarrays: prospects and problems. *Chem Biol* 2001, 8, (2), 105–15. [PubMed: 11251285]
44. Duverger E; Frison N; Roche AC; Monsigny M, Carbohydrate-lectin interactions assessed by surface plasmon resonance. *Biochimie* 2003, 85, (1–2), 167–79. [PubMed: 12765786]
45. Nahalkova J; Svitel J; Gemeiner P; Danielsson B; Pribulova B; Petrus L, Affinity analysis of lectin interaction with immobilized C- and O- glycosides studied by surface plasmon resonance assay. *J Biochem Biophys Methods* 2002, 52, (1), 11–8. [PubMed: 12121750]
46. Niu Y; Jin G, Protein microarray biosensors based on imaging ellipsometry techniques and their applications. *Protein Cell* 2011, 2, (6), 445–55. [PubMed: 21748594]
47. Venkatasubbarao S; Beaudry N; Zhao Y; Chipman R, Evanescent-imagingellipsometry-based microarray reader. *J Biomed Opt* 2006, 11, (1), 014028. [PubMed: 16526905]
48. Sun YS; Zhu X, Real-time, label-free detection of biomolecular interactions in sandwich assays by the oblique-incidence reflectivity difference technique. *Sensors (Basel)* 2014, 14, (12), 23307–20. [PubMed: 25490591]
49. Fei YY; Landry JP; Sun YS; Zhu XD; Luo JT; Wang XB; Lam KS, A novel high-throughput scanning microscope for label-free detection of protein and small-molecule chemical microarrays. *Rev Sci Instrum* 2008, 79, (1), 013708. [PubMed: 18248040]

50. Landry JP; Sun YS; Guo XW; Zhu XD, Protein reactions with surfacebound molecular targets detected by oblique-incidence reflectivity difference microscopes. *Appl Opt* 2008, 47, (18), 3275–88. [PubMed: 18566623]
51. Sun YS; Landry JP; Fei YY; Zhu XD; Luo JT; Wang XB; Lam KS, Macromolecular scaffolds for immobilizing small molecule microarrays in label-free detection of protein-ligand interactions on solid support. *Anal Chem* 2009, 81, (13), 5373–80. [PubMed: 19563213]
52. Sun YS; Lam KS; Zhu XD, Determination of Bovine Serum Albumin Conjugated Drugs by Immobilization as Microarrays and Oblique-Incidence Reflectivity Difference Microscopy. *Instrum Sci Technol* 2014, 42, (4), 475–485.
53. Garrido D; Kim JH; German JB; Raybould HE; Mills DA, Oligosaccharide binding proteins from *Bifidobacterium longum* subsp. *infantis* reveal a preference for host glycans. *PLoS One* 2011, 6, (3), e17315. [PubMed: 21423604]
54. Bode L, Recent advances on structure, metabolism, and function of human milk oligosaccharides. *J Nutr* 2006, 136, (8), 2127–30. [PubMed: 16857829]
55. Ninonuevo MR; Park Y; Yin H; Zhang J; Ward RE; Clowers BH; German JB; Freeman SL; Killeen K; Grimm R; Lebrilla CB, A strategy for annotating the human milk glycome. *J Agric Food Chem* 2006, 54, (20), 7471–80. [PubMed: 17002410]
56. Ninonuevo MR; Perkins PD; Francis J; Lamotte LM; LoCascio RG; Freeman SL; Mills DA; German JB; Grimm R; Lebrilla CB, Daily variations in oligosaccharides of human milk determined by microfluidic chips and mass spectrometry. *J Agric Food Chem* 2008, 56, (2), 618–26. [PubMed: 18088092]
57. Kim JH; An HJ; Garrido D; German JB; Lebrilla CB; Mills DA, Proteomic analysis of *Bifidobacterium longum* subsp. *infantis* reveals the metabolic insight on consumption of prebiotics and host glycans. *PLoS One* 2013, 8, (2), e57535. [PubMed: 23469017]
58. Thomas P; Nabighian E; Bartelt MC; Fong CY; Zhu XD, An obliqueincidence optical reflectivity difference and LEED study of rare-gas growth on a latticemismatched metal substrate. *Appl. Phys. A* 2004, 79, 131–137.
59. Zhu XD, Oblique-incidence optical reflectivity difference from a rough film of crystalline material. *Phys. Rev. B* 2004, 69, 1–5.
60. Majka J; Speck C, Analysis of protein-DNA interactions using surface plasmon resonance. *Adv Biochem Eng Biotechnol* 2007, 104, 13–36. [PubMed: 17290817]
61. Nagata N; Handa H, Real-Time Analysis of Biomolecular Interactions, Applications of BIACORE. Springer-Verlag: Tokyo, Japan, 2000.
62. Sun YS; Zhu XD, Ellipsometry-Based Biosensor for Label-Free Detection of Biomolecular Interactions in Micro array Format. *Sensor Mater* 2013, 25, (9), 673–688.

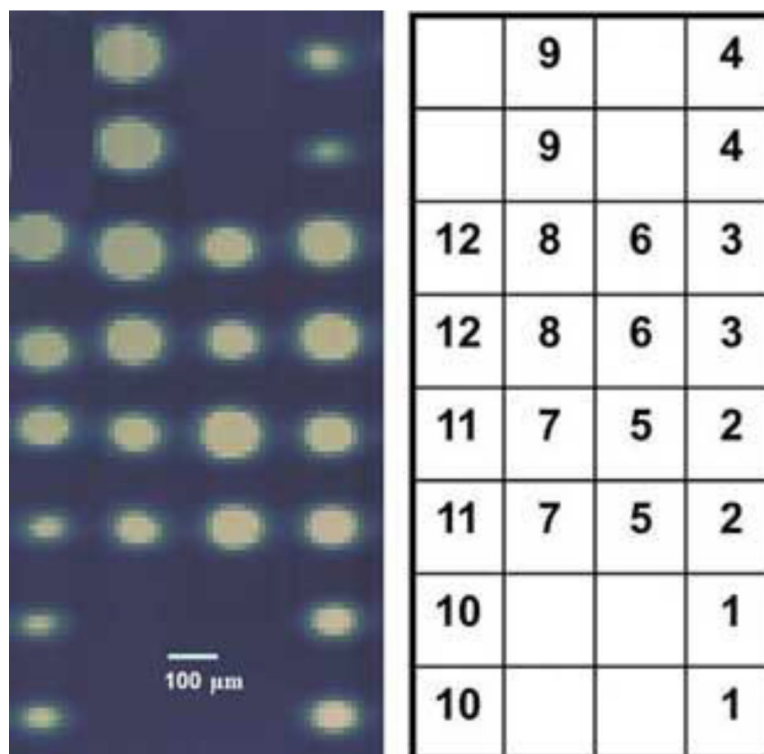


Figure 1.
OI-RD image and corresponding layout of the dry carbohydrate microarray.

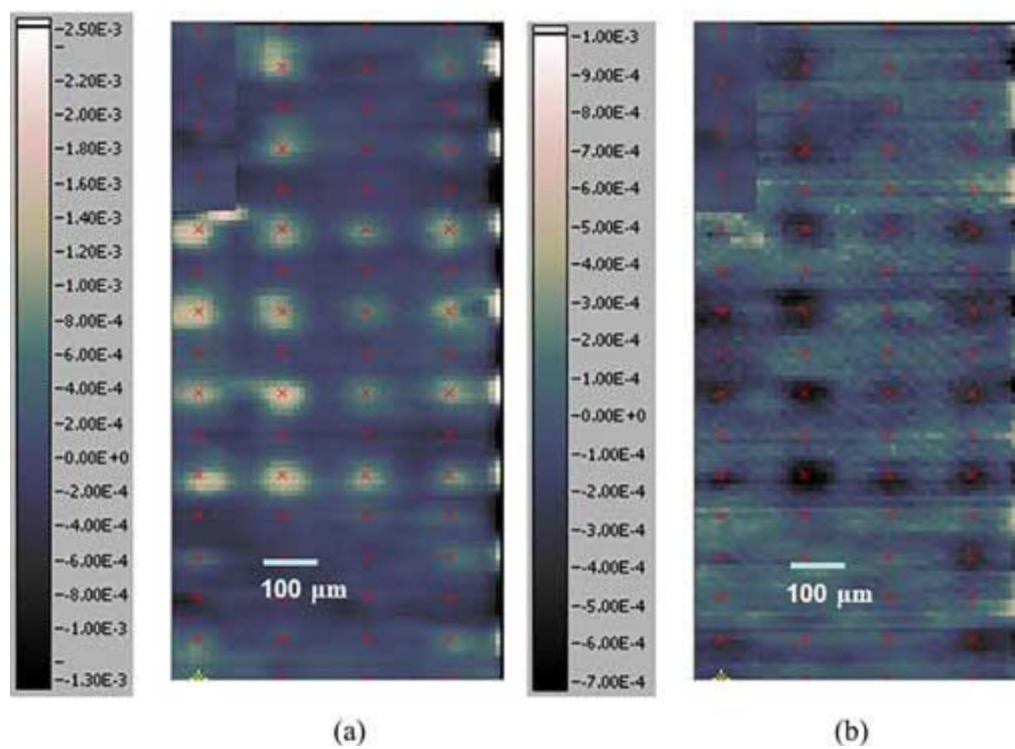


Figure 2.
(a) OI-RD image of the carbohydrate microarray in contact with 1× phosphate buffered saline buffer and (b) differential OI-RD image of the microarray after blocking.

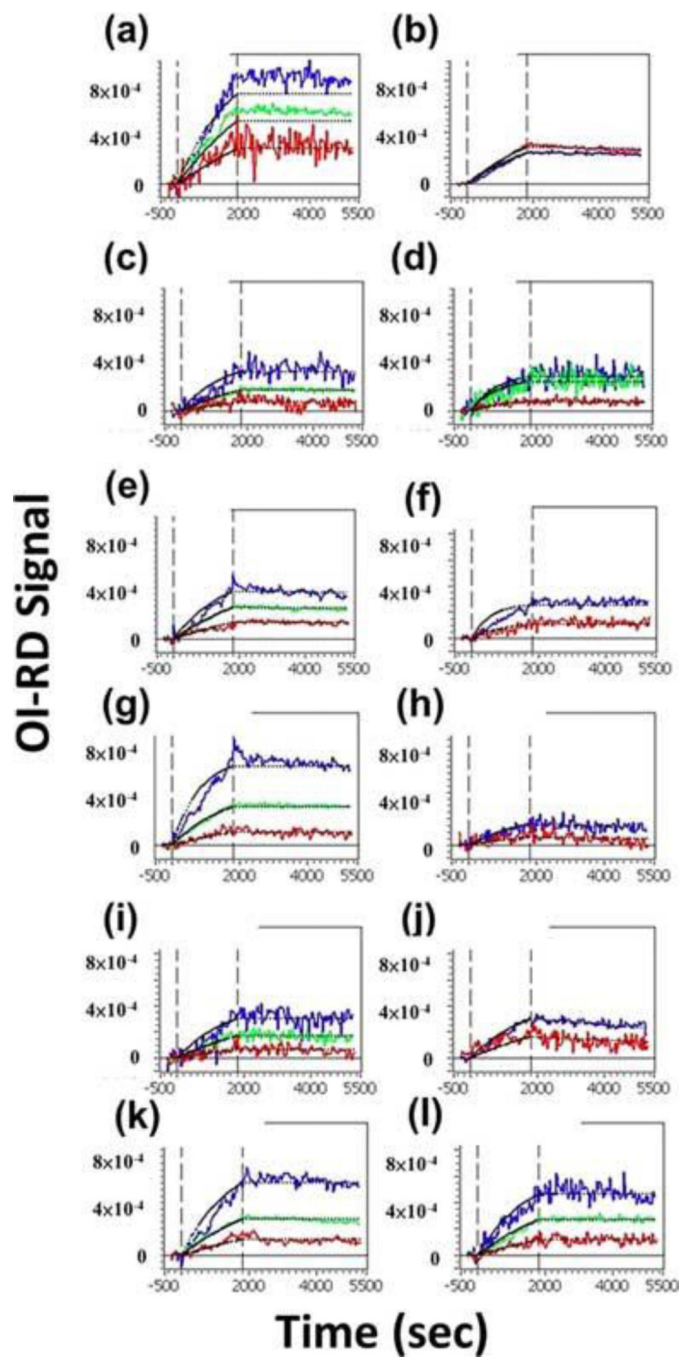


Figure 3. Association-dissociation curves of solute binding protein 2344 reacting with surface-immobilized oligosaccharides: (a) #1; (b) #2; (c) #3; (d) #4; (e) #5; (f) #6; (g) (h) #8; (i) #9; (j) #10; (k) #11; and (l) # 12. The colors indicate different probe concentrations: red: 236 nM; green: 472 nM; and blue: 944 nM.

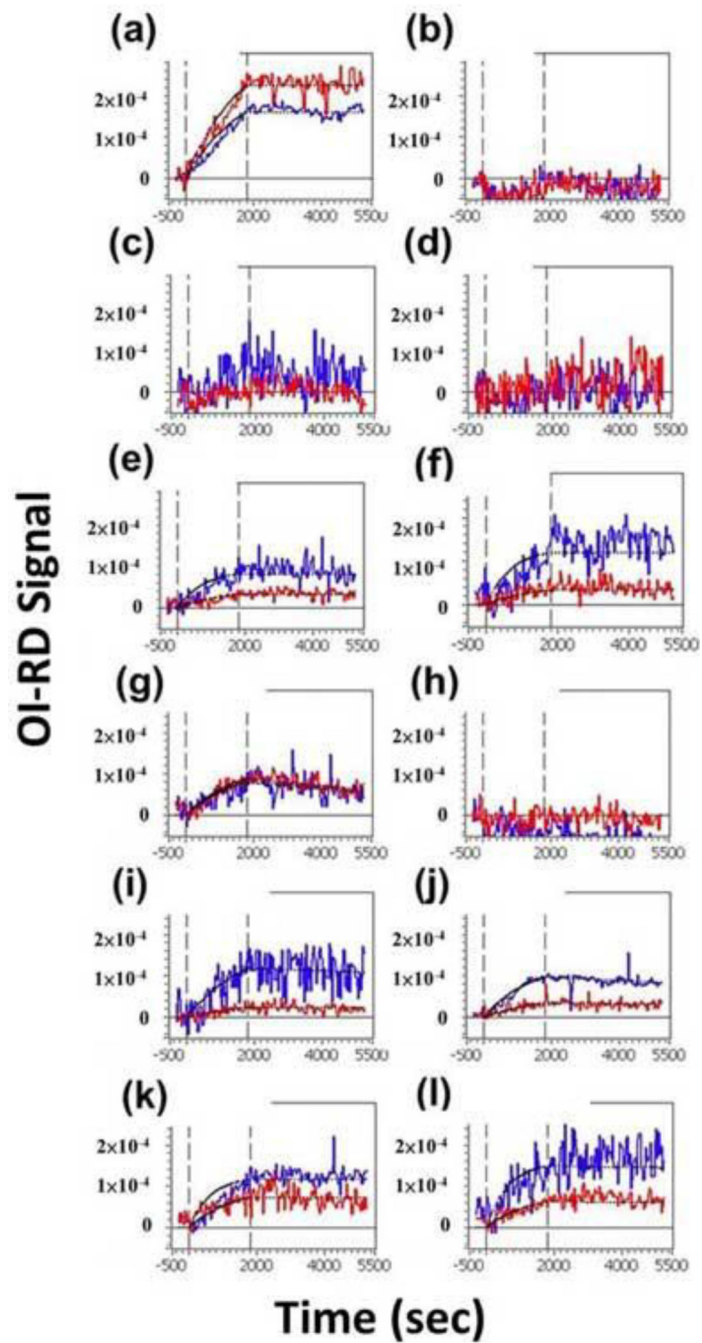


Figure 4. Association-dissociation curves of solute binding protein 2352 reacting with surface-immobilized oligosaccharides: (a) #1; (b) #2; (c) #3; (d) #4; (e) #5; (f) #6; (g) (h) #8; (i) #9; (j) #10; (k) #11; and (l) #12. The colors indicate different probe concentrations: red: 400 nM and blue: 800 nM.

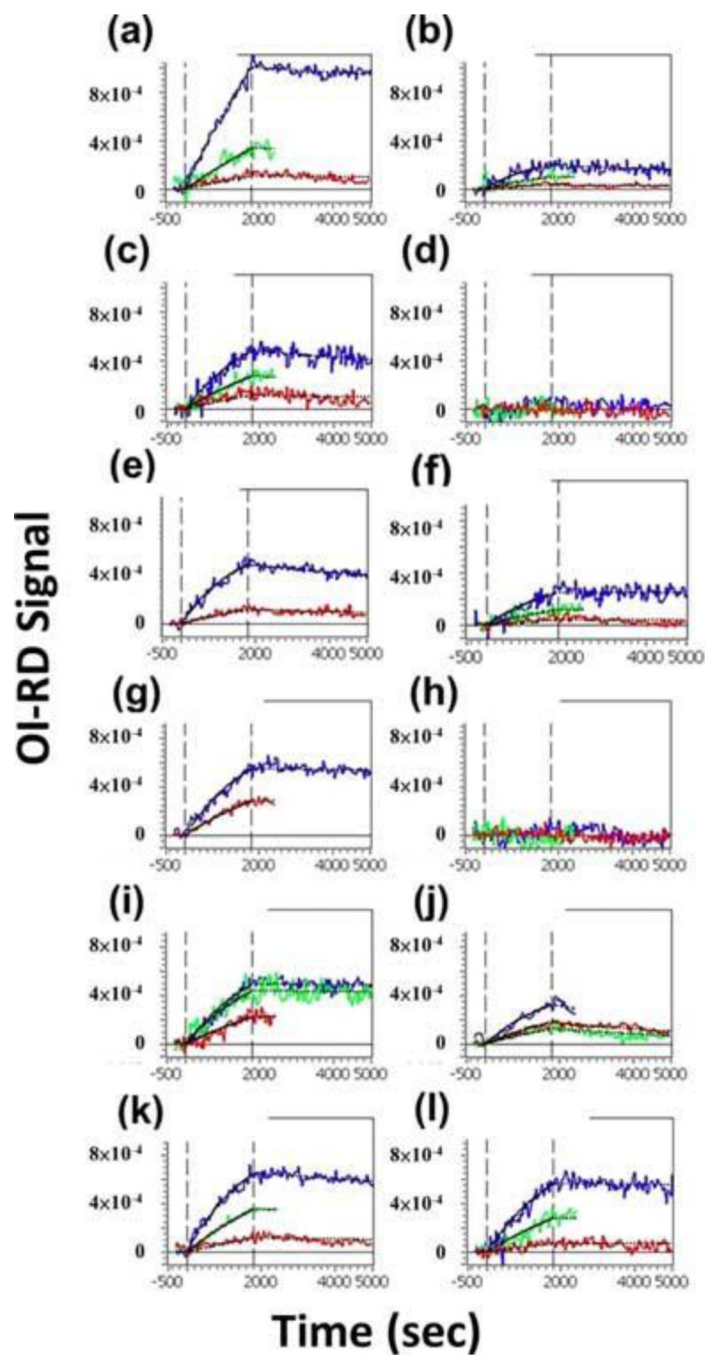


Figure 5. Association-dissociation curves of solute binding protein 2350 reacting with surface-immobilized oligosaccharides: (a) #1; (b) #2; (c) #3; (d) #4; (e) #5; (f) #6; (g) (h) #8; (i) #9; (j) #10; (k) #11; and (l) #12. The colors indicate different probe concentrations: red: 170 nM; green: 340 nM; and blue: 680 nM.

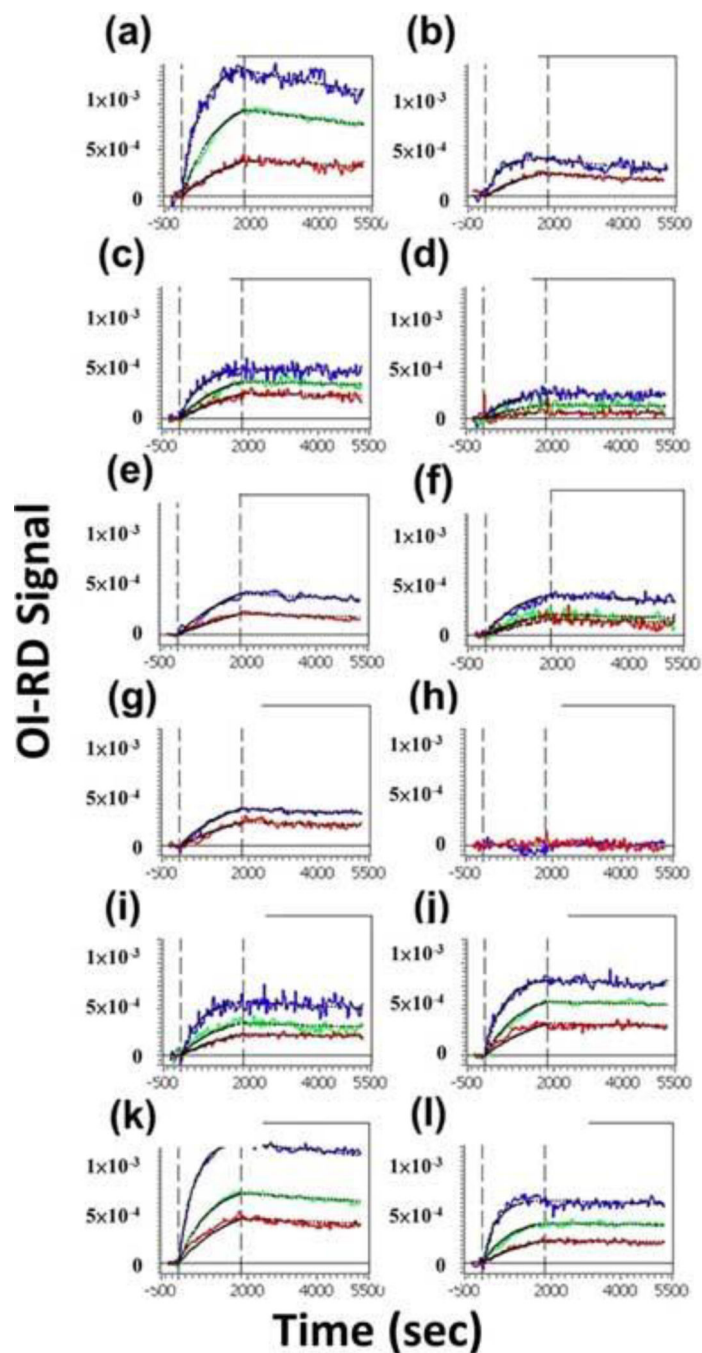


Figure 6. Association-dissociation curves of solute binding protein 0343 reacting with surface-immobilized oligosaccharides: (a) #1; (b) #2; (c) #3; (d) #4; (e) #5; (f) #6; (g) #7; (h) #8; (i) #9; (j) #10; (k) #11; and (l) #12. The colors indicate different probe concentrations: red: 340 nM; green: 680 nM; and blue: 1360 nM.

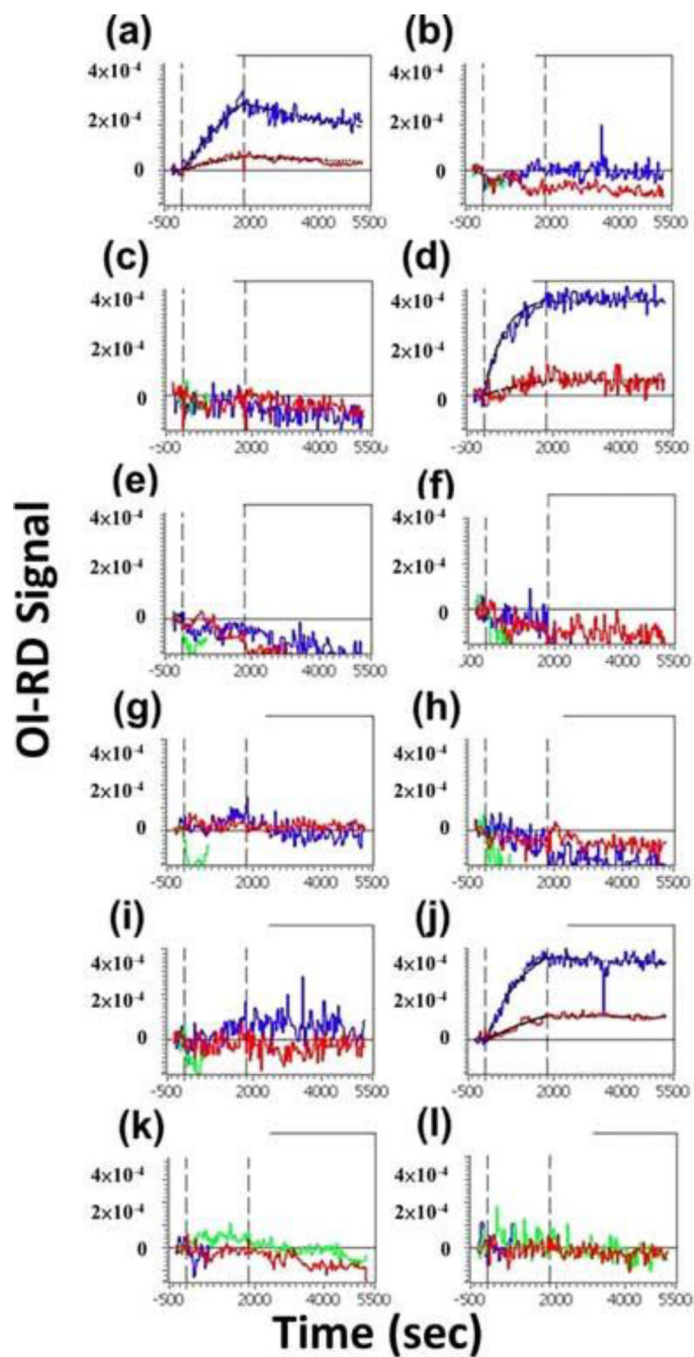


Figure 7. Association-dissociation curves of solute binding protein 2177 reacting with surface-immobilized oligosaccharides: (a) #1; (b) #2; (c) #3; (d) #4; (e) #5; (f) #6; (g) (h) #8; (i) #9; (j) #10; (k) #11; and (l) #12. The colors indicate different probe concentrations: red: 29 nM; green: 57 nM; and blue: 114 nM.

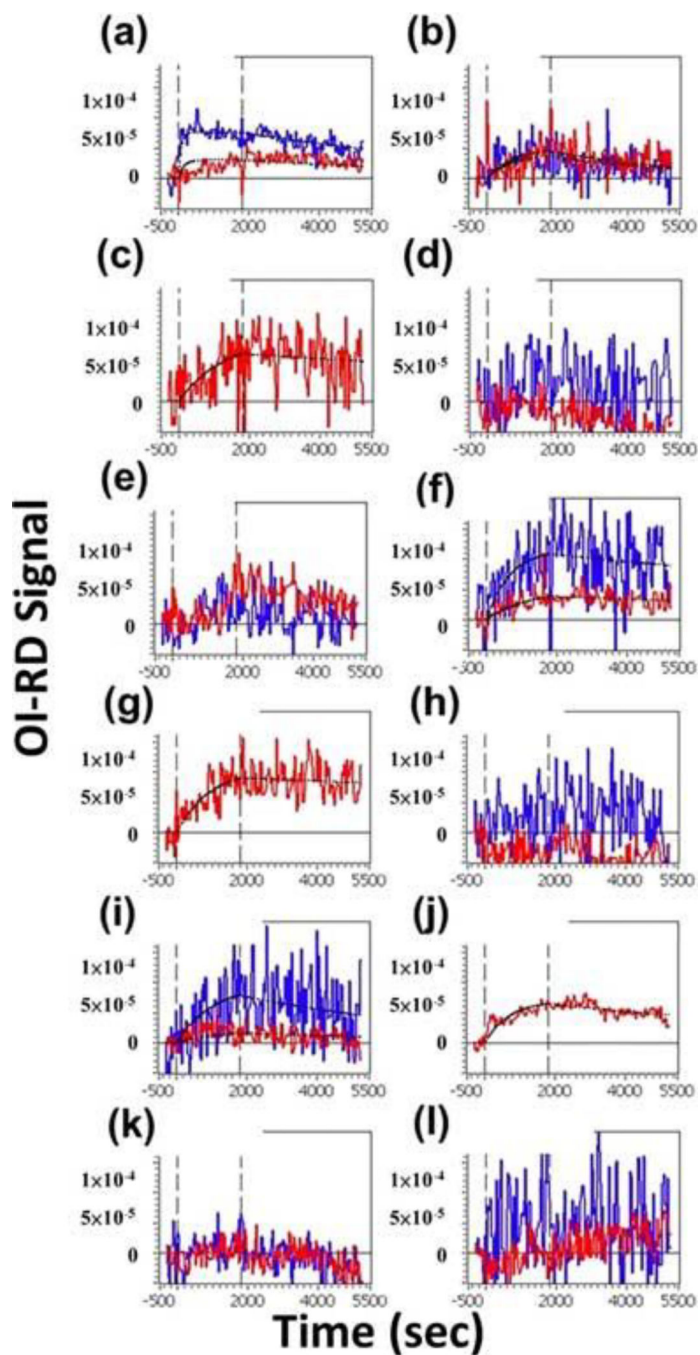


Figure 8. Association-dissociation curves of solute binding protein 0883 reacting with surface-immobilized oligosaccharides: (a) #1; (b) #2; (c) #3; (d) #4; (e) #5; (f) #6; (g) (h) #8; (i) #9; (j) #10; (k) #11; and (l) #12. The colors indicate different probe concentrations: red: 474 nM and blue: 948 nM.

Table 1.

Mass and composition of the aminated oligosaccharides.

Carbohydrate Number	Aminated m/z	Neutral m/z	Number of Hexoses	Number of N-acetylhexose amines	Number of Deoxydexoses	Number of Nacetylneuraminic acids
1	774.3203	707.2484	3	1		
2	920.3782	853.3063	3	1	1	
3	1139.4525	1072.3806	4	2		
4	1285.5104	1218.4385	4	2	1	
5	1577.6262	1510.5543	4	2	3	
6	1650.6426	1583.5707	5	3	1	
7	2161.8327	2094.7608	6	4	2	
8	2307.8906	2240.8187	6	4	3	
9	694.3206	627.2487		3		
10	700.2836	633.2116	2			1
11	1057.3994	990.3275	6			
12	1219.4522	1152.3803	7			

Table 2.

Equilibrium dissociation constants in nM of solute binding proteins binding to carbohydrates. Numbers in the solute binding proteins represent each Family 1 of the solute binding protein locus tag.

Carbohydrate Number (first column)/ solute binding protein (first row)/ equilibrium dissociation constant (nM)	2344	2352	2350	0343	2177	0883
1	<42±2.1	<11.1±0.9	<96.5±5.2	37.4±2.2	69.9±5.1	8.85±1.2
2	22.6±1.5	No reaction	75.2±6.2	52.4±3.2	No reaction	225±10.3
3	<57.7±6.1	No reaction	71±5.2	18.7±2.5	No reaction	62.6±7.1
4	<19.2±1.1	No reaction	No reaction	41.8±3.6	<2.97±0.8	No reaction
5	<15.4±0.9	<17.5±1.2	64.34±8.2	66.7±7.1	No reaction	No reaction
6	<5.97±1.0	<24±3.1	<86.4±7.6	72.1±5.9	No reaction	35.3±4.1
7	<16.3±2.0	148±11.1	12.1±2.0	41.3±3.8	No reaction	26.8±3.0
8	68.7±6.2	No reaction	No reaction	No reaction	No reaction	No reaction
9	<66±5.9	<58.5±6.0	<21.5±1.9	28.6±3.0	No reaction	189±12.9
10	78.7±8.0	51.6±5.8	173±12.2	11.6±2.0	3.26±0.8	35.5±4.1
11	<22.7±2.2	<13.7±2.0	38.4±4.1	19.5±1.4	No reaction	No reaction
12	<30.5±2.5	<13.4±2.1	<70.2±6.5	8.18±1.1	No reaction	No reaction